89Zr-immuno-PET

Jauw, Y.W.S.

2019

document version
Publisher's PDF, also known as Version of record

CHAPTER 2

Radiation dosimetry of ^{89}Zr-labeled chimeric monoclonal antibody U36 as used for immuno-PET in head and neck cancer patients

Pontus K.E. Börjesson
Yvonne W.S. Jauw
Remco de Bree
Jan C. Roos
Jonas A. Castelijns
C. René Leemans
Guus A.M.S. van Dongen
Ronald Boellaard

J Nucl Med 2009; 50:1828-1836

ABSTRACT

Immuno-PET is an appealing concept in tumor detection and planning of antibody-based therapy. For this purpose, the long-lived positron emitter zirconium-89 (t½ = 78.4 h) became recently available. The aim of the present first-in-man ^{89}Zr-immuno-PET study was to assess safety, biodistribution, radiation dose, and quantification of ^{89}Zr-labeled-chimeric monoclonal antibody (cmAb) U36 in patients with head and neck squamous cell carcinoma (HNSCC). In addition, performance of immuno-PET for detecting lymph node metastases was evaluated, as described previously (*1*).

Methods: Twenty HNSCC patients, scheduled to undergo surgical tumor resection, received 75 MBq ^{89}Zr-cmAb U36 (10 mg). Immuno-PET scans were acquired at 1, 24, 72, and/or 144 h p.i. Biodistribution of the radioimmunoconjugate was evaluated by *ex vivo* radioactivity measurement in blood and in biopsies from the surgical specimen obtained 168 h after injection. Uptake levels and residence times in blood, tumors, and organs of interest were derived from quantitative immuno-PET studies and absorbed doses were calculated using OLINDA/EXM 1.0. Red marrow dose was calculated using the residence time for blood.

Results: ^{89}Zr-cmAb U36 was well tolerated by all subjects. PET quantification of blood pool activity in the left ventricle of the heart showed a good agreement with sampled blood activity (mean deviation, 0.2 ± 16.9 %), except for heavy weight patients (> 100 kg). A good agreement was also found for assessment of mAb uptake in primary tumors (mean deviation, -8.4 ± 34.5 %). The mean absorbed red marrow dose was 0.07 ± 0.02 and 0.09 ± 0.01 mSv/MBq in males and females, respectively. The normal organ with the highest absorbed dose was the liver (mean dose of 1.25 ± 0.27 in males and 1.35 ± 0.21 mSv/MBq in females), thereafter followed by kidneys, thyroid, lungs, and spleen. The mean effective dose was 0.53 ± 0.03 mSv/MBq in males and 0.66 ± 0.03 mSv/MBq in females. Measured excretion via the urinary tract was < 3% during the first 72h.

Conclusion: ^{89}Zr-immuno-PET can be safely used to quantitatively assess biodistribution, uptake, organ residence times, and radiation dose. This justifies its further clinical exploitation in tumor detection and planning of mAb-based therapy.

INTRODUCTION

Monoclonal antibodies (mAbs) have been approved for use as diagnostics and therapeutics in a broad range of medical indications, but especially in oncology (*1*). Immuno-PET, the tracking and quantification of mAbs with PET *in vivo*, is an exciting novel option to improve diagnostic imaging and to guide mAb-based therapy *(2-6*).

To enable PET imaging of mAbs , an appropriate positron emitter, with a half-life ($t_{1/2}$) that is compatible with the time needed to achieve optimal tumor-to-nontumor ratios (typically 2-4 days for intact mAbs), has to be securely coupled to the targeting molecule. ^{124}I ($t_{1/2}$ 100.3 h) and ^{89}Zr ($t_{1/2}$ 78.4 h) are particularly suitable in combination with intact mAbs, because their long half-lives allow imaging at late time points for obtaining maximum information. While the non-residualizing positron emitter ^{124}I is particular suitable for immuno-PET when used in combination with non-internalizing intact mAbs, the residualizing positron emitter ^{89}Zr may be optimal in combination with internalizing intact mAbs, since ^{89}Zr stays in the targeted cell ("residualization") after intracellular catabolism of the radioimmunoconjugate (*7*). ^{89}Zr can also be used as a PET surrogate label for prediction of the biodistribution and dosimetry of ^{177}Lu-mAb and ^{90}Y-mAb conjugates as used in radioimmunotherapy trials, although deviations have to be anticipated due to subtle differences in the metal-chelate complexes used (*8,9*).

While first clinical immuno-PET studies with ^{124}I-labeled mAbs have been performed about 15 years ago, technology for ^{89}Zr-immuno-PET became available just recently (*10*). For this purpose, we developed the large scale production of pure ^{89}Zr and a strategy for labeling mAbs with ^{89}Zr via a multi-step synthesis using a succinylated-derivative of desferrioxamine B (Df) as bifunctional chelate (*10*). Labeling technology is universal and, therefore, can be used for each individual mAb or other type of protein. In the mean time, several preclinical immuno-PET studies have been performed with ^{89}Zr-labeled mAbs as prelude to clinical trials, for example with chimeric (mouse/human) mAb (cmAb) U36 (anti-CD44v6) (*10*), DN30 (anti-cMet) (*11*), G250 (anti-carbonic anhydrase IX)(*12*), ibritumomab tiuxetan and rituximab (anti-CD20)(*9*), bevacizumab (anti-VEGF) (*13*), cetuximab (anti-epidermal growth factor receptor)(*8,14*), and trastuzumab (anti-human epidermal growth factor receptor-2)(*15*).

In a first-in-man ^{89}Zr-immuno-PET clinical trial, we recently determined the diagnostic value of immuno-PET with anti-CD44v6 ^{89}Zr-cmAb U36 in patients

with head and neck squamous cell carcinoma (HNSCC), who were at high risk of having neck lymph node metastases. Twenty HNSCC patients underwent ^{89}Zr-cmAb U36 immuno-PET prior to surgery. Immuno-PET detected all primary tumors (n = 17) as well as lymph node metastases in 18 of 25 positive neck levels. It was concluded that for the detection of HNSCC lymph node metastases (and probably distant metastases), immuno-PET with ^{89}Zr-cmAb U36 performs at least as good as CT or MRI.

No radiation dose estimates have been previously described for ^{89}Zr-cmAb U36 or other ^{89}Zr-labeled mAbs. Therefore, the aim of the present study was to assess safety, biodistribution, radiation dose, and the potential for quantification of immuno-PET with ^{89}Zr-cmAb U36 in HNSCC patients using data of aforementioned clinical trial.

MATERIALS AND METHODS

Patient Study

Twenty patients (8 females and 12 males) with histologically proven HNSCC (Table 1), at high risk of having neck lymph node metastasis and, therefore, planned to undergo neck dissection with or without resection of the primary tumor, participated in this study. Other eligibility criteria have been decribed previously (*2*). Patients received cmAb U36 IgG radiolabeled with ^{89}Zr (74.9 ± 0.6 MBq). The total administered cmAb U36 dosage was 10 mg for all patients. In previous studies, it had been demonstrated that biodistribution is not mAb dose dependent within the range 2 - 52 mg (*16,17*). Surgery was performed 6-8 days after administration of radiolabeled cmAb U36.

Safety

Prior and up to 6 wk after administration of radiolabeled cmAb U36, routine laboratory analyses were performed, including hemoglobin, hematocrit, mean corpuscular volume, red blood cell count, white blood cell count (including automated differential), platelet count, sodium, potassium, calcium, chloride, creatinine, urea, uric acid, alanine aminotransferase, aspartate aminotransferase, alkaline phosphatase, gamma glutamyl transferase, albumin, glucose, bilirubin, thyroid stimulating hormone, and urine sediment. Vital signs including pulse rate, blood pressure, temperature, and respiratory rate were recorded before and up to

3 h post-injection (p.i.). On the basis of previous studies with anti-CD44v6 mAbs, cmAb U36 included, no adverse effects had to be expected (*17*). Dose rates (μSv/h) were measured at 1, 24, and 72 h p.i. at a distance of 100 cm with a γ-radiation dose rate counter (Berthold LB 1230 EG&G, Wildbad, Germany). In addition, human anti-cmAb U36 and anti-Df-cmAb U36 antibody responses were assessed (*2*).

Table 1. Patient and tumor characteristics

Patient	Sex	Age	Weight (kg)	Primary tumor	cTNM	pTNM
1	F	57	68	Oral cavity, tongue, right	T2N0M0	T2N1M0
2	M	57	82	Oropharynx, base of tongue, right	TXN2aM0	T1N2bM0
3	F	72	71	Oropharynx, tonsil, right	T2N2bM0	T2N2bM0
4	F	53	81	Oropharynx, tonsil, right	T3N0M0	T3N2bM0
5	M	63	78	Oropharynx, tonsil, right	T4N0M0	T4N2bM0
6	F	58	62	Oral cavity, floor of mouth, left	T4N0M0	T4N2bM0
7	M	54	67	Oral cavity, tongue, right	T3N0M0	T3N2bM0
8	M	55	72	Oropharynx, tonsil, left	T4N2aM0	T4N2bM0
9	F	54	82	Hypopharynx, piriform sinus, left	T4N2bM0	T4N2bM0
10	F	65	67	Oral cavity, base of tongue, right	T2N0M0	T2N0M0
11	M	53	90	Larynx, glottic	T4N0M0	T4N0M0
12	M	59	75	Larynx, supraglottic	T4N0M0	T4N0M0
13	F	49	49	Residual disease of T2N0 tonsil carcinoma, left	NA	NA
14	M	58	100	Oropharynx, base of tongue, right	T2N2bM0	T2N2bM0
15	M	48	115	Oropharynx, tonsil, right	T3N0M0	T3N1M0
16	F	63	67	Oropharynx, tonsil, left	T3N2bM0	T3N2cM0
17	M	53	104	Oropharynx, tonsil, right	T2N3M0	T2N3M0
19	M	71	87	Oropharynx, soft palate, right	T3N2cM0	T2N2cM0
20	M	60	58	Larynx, supraglottic, recurrence	NA	NA

Abbreviations: NA, not applicable

Monoclonal antibody U36

Selection and production of mouse mAb (mmAb) U36 and its chimeric IgG1 derivative cmAb U36 have been described previously (*17*). mAb U36 binds to the v6 region of CD44 (CD44v6). Expression of CD44v6 was found to be abundant and homogenous in 96% of all primary HNSCC and HNSCC lymph node metastases (*18*). In normal tissues, expression has been found in epithelial tissues such as skin, breast and prostate myoepithelium, and bronchial epithelium (*19*). CD44v6 has been suggested to be involved in tumor formation, tumor cell invasion, metastasis formation, and cancer cell stemness *(20,21)*.

Synthesis of ^{89}Zr-cmAb U36

The synthesis and purification of ^{89}Zr, its coupling to cmAb U36 via the chelate Df (Desferal®, Novartis Pharma AG, Basel, Switzerland), as well as the procedures and results of quality tests, have been described previously (*2*). ^{89}Zr emits positrons with a main energy of 897 keV and an abundance of 22.7%. In addition, non-prompt 909 keV photons are emitted at an abundance of 99.9%.

Pharmacokinetics

Serial blood samples were taken from a peripheral vein of the arm opposite the infusion site for determination of activity at the following time points: 5, 10, and 30 min, and 1, 2, 4, 16, 21, 72, and 168 h after completion of infusion. Urine was collected in intervals 0-24, 24-48, and 48-72 h p.i. to determine renal excretion of ^{89}Zr. Aliquots of blood, plasma, and urine samples were measured for ^{89}Zr activity in an isotope well-counter (1470 Wizard, Wallac, Turku, Finland), compared to an aliquot retained from the conjugate preparation, and corrected for decay. Blood activity was expressed as the percentage of the injected dose per kg (%ID/kg).

PET acquisition

PET scans were obtained at 1 h (all patients, except no 4 and 16), 24 h (patients 1-6), 72 h (all patients) and/or 144 h (all patients, except no 1, 2, and 13) after intravenous injection of ^{89}Zr-cmAb U36, using a dedicated full ring PET scanner (ECAT EXACT HR+, CTI/Siemens, Knoxville, TN, USA) as described before *(2)*. Prior to this study, the PET scanner was calibrated using a standard cylindrical calibration phantom filled with a 5 kBq/cm^3 ^{89}Zr solution. This calibration was performed to verify the quantitative accuracy of the scanner in the presence of 909 keV gamma photons emitted by ^{89}Zr and the impact of emission spillover into the transmission scans. This procedure indicated that activity concentrations measured with the HR+ were accurate within 5%. During image reconstruction all scans were normalized and corrected for randoms, scatter, attenuation, and decay. Reconstructions were performed using an attenuation and normalization weighted ordered subset expectation maximization (OSEM) algorithm (ECAT software version 7.2, CTI/Siemens) with 2 iterations and 16 subsets followed by post-smoothing of the reconstructed image using a 5-mm FWHM Gaussian filter. Due to the low amount of radioactivity administered to the patients (for radiation exposure reasons), images with attenuation correction showed high noise levels. Therefore, OSEM reconstructions without attenuation (and thus scatter) correction were performed as well and used for visual interpretation only.

Validation of quantitative ^{89}Zr-immuno-PET imaging

OSEM reconstructions with attenuation correction of the immuno-PET scans were used to investigate the accuracy of quantification ^{89}Zr-cmAb U36 PET *in vivo*. To this end, three 1.5 cm diameter 'regions of interest' (ROIs) were defined within the left ventricle of the heart in three subsequent image planes using an axial view of the PET images. The average activity concentration within these ROIs, representing PET assessed bloodpool activity concentration, were directly compared with the activity concentration measured in manual blood samples ("sampled blood activity") using a calibrated well counter in order to validate the quantitative accuracy of ^{89}Zr-PET *in vivo*.

In addition, the uptake of the radioimmunoconjugate in tumors (%ID/cm^3) as assessed from scans acquired at 144 h p.i., was compared with the uptake (%ID/g) derived from tumor biopsies collected at 168 h p.i. %ID/cm^3 as derived from the PET scans was converted to %ID/g using a soft tissue density factor of 1.04 g/cm^3.

VOI definition

The uptake in different organs was determined by manually defined ROIs using the Clinical Application Programming Package (CAPP, provided with the ECAT software). ^{89}Zr uptake was determined in the following organs: lung, liver, spleen, kidney, heart, and if visible, thyroid. In addition, a semi-automatic 'volume of interest' (VOI) was defined over the tumor using in-home developed software tools (*22*).

Details of ROI/VOI definition: As most organs could be visually best identified on the 1 h p.i. emission scans, most organ 3D VOIs were defined manually using this early uptake scan. However, VOIs for the thyroid and tumor were defined on the last scan, because their delineation was optimal at this last time point. Finally, lung regions were defined on reconstructed transmission scans, using the semi-automatic isocontour tool within the CAPP software. All 3D VOIs were defined using a coronal view of the PET images.

A 3D VOI was generated from multiple 2D ROIs by grouping these ROIs into the VOI. The ROIs on the first and last slices were not used for the VOIs, since these were prone to partial volume effects (spill-in and spill-out) and/or sampling errors. The VOIs defined on the 1 h p.i. scan were saved and imported to the other time frames, where the organs were not as clearly visible. To allow for projection of VOIs onto scans obtained at other time intervals, patients were scanned in the

same (patient and bed) position during subsequent studies, by using rigid head immobilization devices (e.g. radiotherapy mask) and belts around the patient. To ensure correct positioning of the VOIs, the elevation of the bed was registered for all scans and in case of differences in patient or bed position, scans were aligned using in home-developed software program. Furthermore, in case of remaining dislocation of VOIs, all VOIs were relocated in one step to keep the internal relations intact. For relocation, the alignment of lungs VOIs and the contour of the head and neck were verified using reconstructed transmission scans (for each subsequent study) as well. However, if still necessary, VOIs were ungrouped and individual VOIs were relocated to improve the position. After this VOI positioning procedure all VOIs were saved and projected onto the emission scans. The mean uptake in Bq/cm^3 was then derived using these final VOIs.

The tumor was defined on 144 h p.i. scan using a tool, which semi-automatically defined a 3D 50% (to max) isocontour around the tumor, and next the mean uptake in Bq/cm^3 was calculated. The mean tumor uptake was determined for the latest acquired PET study only, as correct repositioning of the tumor VOI onto earlier scans could not be reliably visually verified due to lack of signal from the tumor.

All VOIs set on organs and tumors, were evaluated by 2 experienced nuclear physicians.

Internal radiation dosimetry

The internal radiation dosimetry for the adult human was evaluated through the normalized cumulated activities for each patient provided as input to the OLINDA/EXM 1.0 code (*23*).

Residence times were calculated for liver, kidneys, lungs, spleen, and the remainder of the body, entering the percentage of the injected dose at each time point for each patient in OLINDA/EXM 1.0 and fitting these data using a mono-exponential function. The residence times for the thyroid were calculated using trapezoidal integration. The remaining area under the curve from the end of data collection until infinity was determined by considering physical decay only. The residence time of the remainder of the body was defined as: 113 - sum of residence times of source organs. A total residence time for the entire body of 113 h is obtained in case of no biological clearance. Red marrow dose was estimated using sampled blood clearance data (*24,25*). The red marrow concentration was assumed to be 30% of the blood activity concentration (conversion factor = 0.3). In addition, the dose from the remainder of the body onto red marrow was considered as well.

RESULTS

Unless otherwise specified, all ^{89}Zr activities are decay corrected to time of injection. For 1 patient (patient 18) imaged, not enough data were available for adequate dosimetric analysis. Regarding the evaluation of ^{89}Zr-immuno-PET imaging to quantify tumor uptake, 4 patients (patients 1, 2, 13, and 18) were excluded from analysis because the lack of a scan at 144 h p.i. Another patient (patient 6) was excluded because of delayed surgery 2 wk p.i.

Safety

^{89}Zr-cmAbU36 was found to be safe and well tolerated in all subjects. Neither adverse reactions nor significant changes in earlier mentioned blood and urine parameters were observed, that could be related to the study drug. The mean radiation dose rates measured 1, 24, and 72 h p.i. at a distance of 100 cm were 7.0 ± 0.3, 5.7 ± 0.3 and 3.8 ± 0.2 μSv/h, respectively. Patient 9 and 10 developed a human anti-chimeric antibody (HACA) response, and elevated titers were found at 1 and 6 wk p.i., irrespective whether cmAb U36 IgG or ^{89}Zr-*N*-sucDf-cmAb U36 was used in the ELISA. These data indicate that the response was directed to the protein part of the conjugate and not to the *N*-sucDf chelate attached to the cmAb.

Biodistribution

Images of a representative male patient between 1 and 144 h after injection of ^{89}Zr-cmAbU36 are presented in Figure 1. Whole body images obtained directly after administration of ^{89}Zr-cmAb U36 showed mainly blood-pool activity with delineation of the heart, lungs, liver, kidneys, spleen and nose. Uptake of radioactivity for most organs decreased over time, while increased uptake was only seen at tumor sites and in the thyroid of some of the patients (patients 1, 6, 7, 10, and 11).

The estimated uptake of ^{89}Zr-cmAbU36 in single organs, is presented in Table 2. The visual quality of the immuno-PET images varied between different patients. Figure 2 illustrates the difference in visual quality between an average weight patient (58 kg) and an obese patient (104 kg).

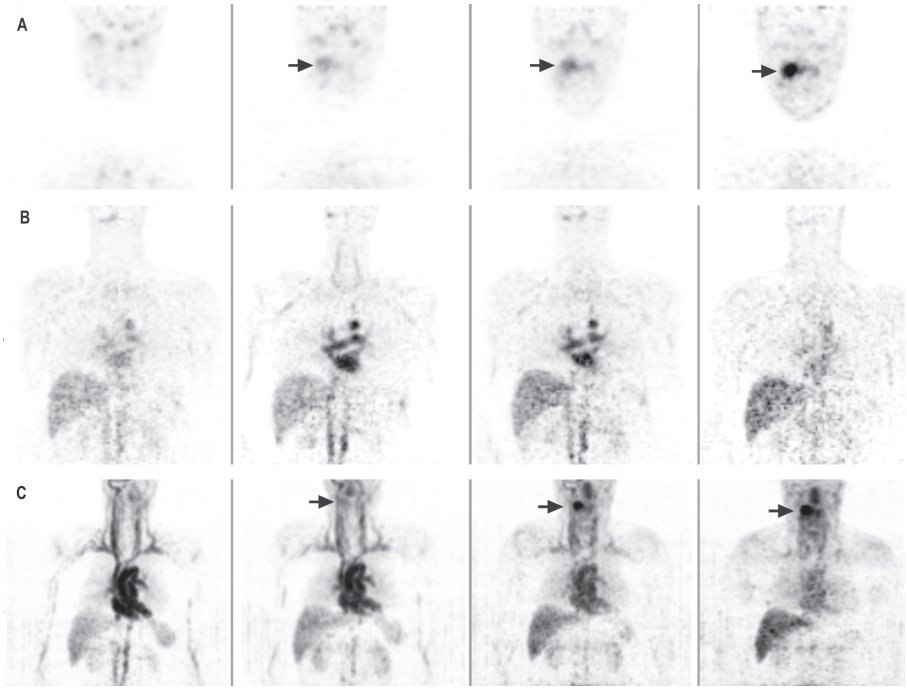

Figure 1. Representative coronal images of male patient with an oropharyngeal tumor, left to right arranged from 1, 24, 72, and 144 h p.i. A: shows the increased uptake in time of ^{89}Zr-cmAb U36 in tumor. B: shows circulating ^{89}Zr-cmAb U36 in the heart and uptake in organs. C: maximum intensity projections of the same patient as shown in A and B. Note that grayscale settings were set for each image independently for clarity reasons.

Table 2. Uptake of ^{89}Zr-cmAbU36 in single organs

	Males (mean %ID ± SD)			
Organ	t = 0 h	t = 24 h	t = 72 h	t = 144 h
Kidneys	1.21 ± 0.23	1.36 ± 0.14	0.70 ± 0.16	0.26 ± 0.09
Liver	12.23 ± 2.12	11.98 ± 0.78	6.18 ± 1.44	2.83 ± 0.79
Lungs	4.51 ± 3.58	5.86 ± 1.30	1.84 ± 1.20	0.69 ± 0.47
Spleen	0.99 ± 0.27	0.75 ± 0.12	0.29 ± 0.10	0.10 ± 0.04
Thyroid	0.08 ± 0.02	0.11	0.07 ± 0.04	0.05 ± 0.02
	Females (mean %ID ± SD)			
Kidneys	1.78 ± 0.34	1.69 ± 0.44	0.95 ± 0.27	0.37 ± 0.07
Liver	11.50 ± 2.45	7.98 ± 1.02	4.94 ± 0.95	2.36 ± 0.52
Lungs	5.91 ± 1.94	3.86 ± 1.52	2.52 ± 0.75	1.16 ± 0.29
Spleen	1.02 ± 0.36	0.72 ± 0.09	0.27 ± 0.12	0.10 ± 0.05
Thyroid	0.06 ± 0.03	0.06 ± 0.04	0.10 ± 0.03	0.05 ± 0.03

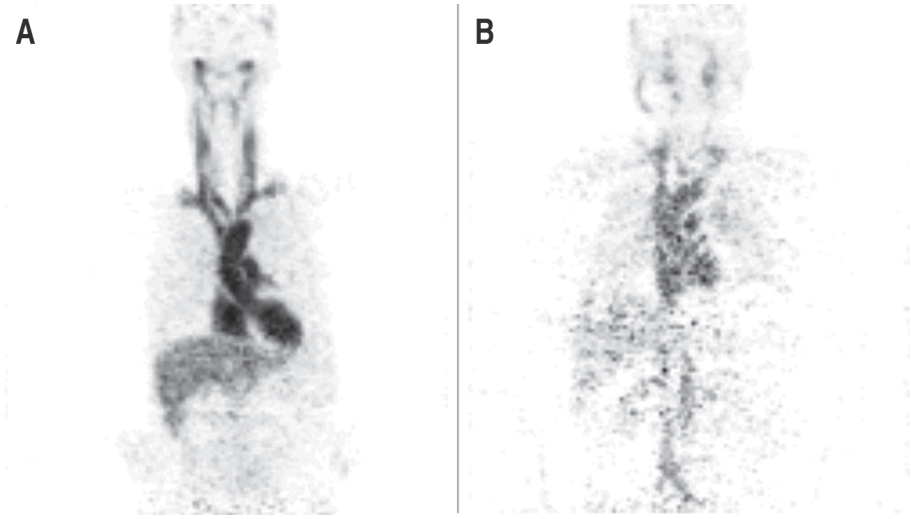

Figure 2. Illustration of the difference in visual quality of coronal PET images obtained 1 h after injection of ^{89}Zr-cmAb U36 between A: an average weight patient (58 kg) and B: an obese patient (104 kg).

PET derived bloodpool activity vs sampled blood

Variation in visual image quality also affects the quantitative analysis of the ^{89}Zr-cmAbU36 immuno-PET images in a proportion of patients, as shown in Figure 3. This plot depicts the percentage under- and overestimation of the blood activity as assessed by immuno-PET. To this end, immuno-PET derived activity in the left ventricle of the heart was compared to activity in sampled blood. Patients with a weight lower than 100 kg showed in general a good agreement with manually sampled data (mean deviation 0.2 ± 16.9%). Patients above 100 kg showed an underestimation of activity by immuno-PET, especially for later time images.

Figure 4 shows blood kinetics, either assessed by immuno-PET or by blood sampling, for the whole group of evaluable patients (n=19). For the group of patients as a whole, no statistically significant ($P = 0.503$) differences were observed between the two methods used for assessment of activity. In addition, the small variances suggest a consistency of the pharmacokinetics in these patients, also for patients who developed a HACA response. Therefore, we decided to use data of all these patients for radiation dose estimations.

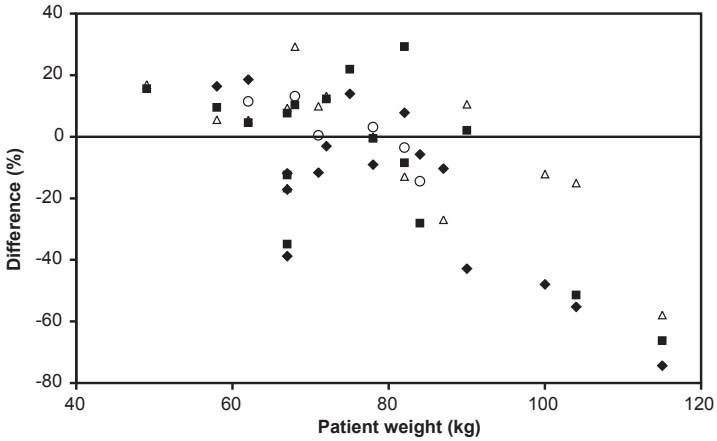

Figure 3. Difference between PET assessed blood pool activity and sampled blood activity of ^{89}Zr-cmAb U36 as function of patient weight. Difference in activity was assessed at 1 h (Δ), 24 h (○), 72 h (■), and 144 h (♦) after injection.

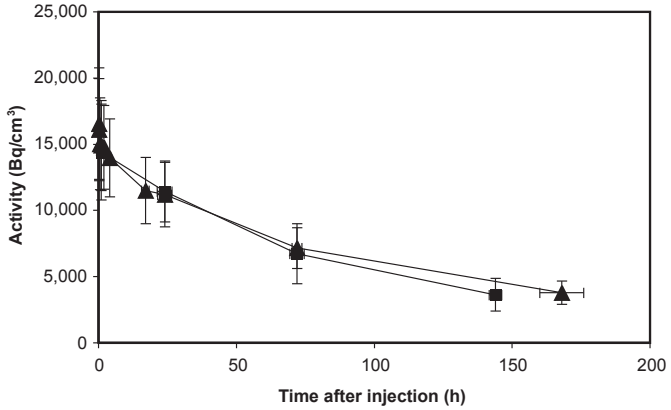

Figure 4. Mean ^{89}Zr-cmAb U36 activity in blood (Bq/cm^3) of the study population: PET assessed bloodpool activity within the left ventricle of the heart (■), and sampled bloodpool activity (▲).

Quantification of mAb uptake in tumors

Antibody uptake was assessed on 144 h p.i. scans for all primary tumors, and compared with uptake data from biopsies obtained 168 h p.i. Comparison of %ID/g derived from biopsy data and PET data, respectively, showed a good agreement with slightly lower values for PET (mean deviation -8.4 ± 34.5%). The mean tumor uptake at 168 h p.i. as assessed by biopsies appeared to be 0.019 ± 0.010 %ID/g (range 0.006 - 0.038 %ID/g).

Red marrow doses

The doses absorbed in the red marrow were estimated in 19 patients, as presented in Table 3. The mean red marrow dose was 0.07 ± 0.02 mSv/MBq in males and 0.09 ± 0.01 mSv/MBq in women.

Table 3. Absorbed doses in red marrow

Patient no.	Red marrow dose* (mSv/MBq)
Males	
2	0.07
5	0.07
7	0.06
8	0.06
11	0.08
12	0.07
14	0.09
15	0.11
17	0.09
19	0.07
20	0.05
Mean ± SD	0.07 ± 0.02
Females	
1	0.09
3	0.10
4	0.11
6	0.09
9	0.11
10	0.09
13	0.07
16	0.09
Mean ± SD	0.09 ± 0.01

* Conversion factor = 0.3

Absorbed doses in source organs and whole body

Residence times of the source organs were entered into the OLINDA/EXM 1.0 program. The results of the OLINDA/EXM 1.0 analysis are listed in Table 4. The effective dose for each patient was calculated using the available organ dosimetry data of the source organs. Excretion of ^{89}Zr via the urinary pathway was 2.59 ± 1.89 %ID during the first 72 h after injection. As there is also very little activity seen in the intestines, most loss of radioactivity is due to physical decay. The mean effective dose for the whole body was 0.53 ± 0.03 mSv/MBq in males and 0.66 ± 0.03 mSv/MBq in females. As an alternative, the effective dose was also calculated by considering the body to be a homogenous mass, i.e. ignoring organ doses and

assuming a residence time of 113 h for the entire patient. This simplified procedure showed only a minor decrease of the estimated effective dose: 0.44 ±0.002 mSv/MBq in males and 0.54 ± 0.002 mSv/MBq in females. Difference in estimated effective dose between males and females, with versus without ignoring the biodistribution, suggests that this difference might be explained by use of different models (male versus female) within OLINDA/EXM 1.0.

The normal organs with the highest absorbed dose were the liver (mean dose in males 1.25 ± 0.27 mSv/MBq; in females 1.35 ± 0.21 mSv/MBq) and kidneys (mean dose in males 0.82 ± 0.15 mSv/MBq; in females 1.18 ± 0.26 mSv/MBq).

Table 4. Absorbed organ doses

	Organ dose (mSv/MBq)						Effective dose (mSv/MBq)
Patient no.	Kidneys	Liver	Lungs	Spleen	Thyroid	Total body	Organ dosimetry
Males							
2	1.01	1.60	0.93	0.74	1.28	0.45	0.60
5	0.85	1.47	0.83	0.66	NV	0.45	0.54
7	0.86	1.20	0.68	0.74	0.70	0.44	0.53
8	0.84	1.17	1.01	0.71	NV	0.44	0.55
11	0.96	1.48	0.54	0.81	1.40	0.45	0.56
12	1.01	1.55	0.53	0.82	NV	0.45	0.52
14	0.73	1.01	0.44	0.58	0.86	0.44	0.52
15	0.69	1.23	0.50	0.57	0.70	0.44	0.52
17	0.58	0.69	0.42	0.47	0.72	0.44	0.49
19	0.80	1.14	0.54	0.59	0.85	0.44	0.52
20	0.64	1.23	0.49	0.70	0.81	0.44	0.52
Mean ± SD	0.82 ± 0.15	1.25 ± 0.27	0.63 ± 0.20	0.67 ± 0.11	0.91 ± 0.27	0.44 ± 0.0022	0.53 ± 0.03
Females							
1	1.26	1.31	0.63	0.89	1.12	0.54	0.64
3	1.12	1.19	0.84	0.86	NV	0.54	0.65
4	0.87	1.15	0.96	0.62	NV	0.54	0.63
6	1.32	1.56	1.01	0.87	0.93	0.55	0.67
9	0.99	1.65	1.11	0.86	NV	0.55	0.66
10	1.04	1.09	1.05	0.84	1.44	0.54	0.69
13	1.71	1.52	1.12	0.64	1.11	0.55	0.71
16	1.15	1.33	0.83	0.55	0.98	0.54	0.65
Mean ± SD	1.18 ± 0.26	1.35 ± 0.21	0.94 ± 0.17	0.77 ± 0.14	1.12 ± 0.20	0.54 ± 0.0024	0.66 ± 0.03

Abbreviations: NV, not visible

DISCUSSION

The purpose of this study was to assess the safety, and to evaluate the biodistribution, the radiation dose, and the potential for quantification of immuno-PET with ^{89}Zr-labeled-chimeric mAb (cmAb) U36 in HNSCC patients. In this study, the tracer was found to be safe and well tolerated. No adverse events occurred. A HACA response was only seen in two patients, while none of the antibody responses was directed to the chelate. In all normal organs, the uptake of radioactivity decreased in time. Only in the tumor and in a few patients in the thyroid, uptake increased in time, suggesting specific uptake of ^{89}Zr-cmAb U36. Such variable and sometimes high thyroid uptake was previously observed in head and neck cancer patients who had been injected with ^{99m}Tc-cmAb U36 (*16*). This might indicate that in some individuals CD44v6 is expressed in the thyroid.

Furthermore, the advantage of the more detailed images obtained with ^{89}Zr-immuno-PET is the possibility of non-invasive quantification. In the majority of the images the visual quality was acceptable for defining ROI's, but there was a variation between images of different patients and in some images the delineation of organs and tumor was suboptimal. Nevertheless, quantification results seem plausible. The ^{89}Zr calibration procedure indicated that the quantitative accuracy of the scanner was not compromised by the presence of 909 keV gamma photons emitted from ^{89}Zr and due to emission spillover into the transmission scans. In fact, the procedure was repeated for activity concentrations of about 17 kBq/cc (111 MBq in a phantom of 6283 ml) showing that quantitative accuracy was not affected at higher count rates as well. Although the 909 keV photons could have resulted in increased dead time and randoms fraction, the ^{89}Zr activity in the field of view is much lower than usually applied for e.g. FDG studies (up to 370 MBq FDG for patients and about 70 MBq FDG in a 6 L phantom for calibrations). Moreover, the 511 keV photon flux from ^{89}Zr is much lower than that seen in FDG studies due to lower positron emission abundance compared with ^{18}F. Another effect that could hamper quantification might be emission spillover into the transmission scan. However, emission spillover into the transmission scan is minimized in two ways. First, transmission scans are based on coincidence counting of the 511 keV photons emitted by the ^{68}Ge transmission rod sources, thereby reducing the detection of non-coincident emitted photons (although these still result in increased randoms fraction). Second, during transmission scanning a "rod windowing" technique is applied (*26*). Rod windowing discards all detected

coincidences that do not intersect the rod source (within a certain distance) and, as such, it reduces the influence of scatter, randoms, and emission spillover. To further validate quantitative accuracy, a comparison was made between blood pool activity seen in the PET scanner versus those in manual samples.

Quantification of blood pool activity in the left ventricle of the heart showed good agreement with the sampled blood activity, except for a few heavy weight patients (> 100 kg). This suggests that immuno-PET with ^{89}Zr-cmAb U36 can be used to quantify the radiation dose of the whole body and normal organs of interest. However, as earlier shown with FDG-PET, excessive body weight has negative effects on both quantitative and qualitative scan analysis (*27-30*). For ^{89}Zr studies these effects may be even more pronounced due to the low positron emission abundance resulting in lower noise equivalent count rates (NECR) than seen with FDG studies. The low NECR could potentially hamper the accuracy and precision of the scatter correction, but further studies are required to fully understand the negative bias seen with heavier patients. Yet the association between patient weight and bias suggests that this effect is indeed related to scatter correction issues. Despite this fact, a good agreement between PET and sample derived blood pool activities was seen for most other scans and subjects (Figure 3). Note that in future studies, with the use of modern PET/CT-scanners in combination with time-of-flight reconstruction and optimalized scan protocols, it is probable that these problems will be of less magnitude, but this would require further validation as well.

Also in the assessment of tumor uptake, a good agreement was found between PET derived data and data obtained from biopsies, despite there was one day difference in assessment time (144 h p.i. versus 168 h p.i.). This good agreement is quite remarkable since both methods are prone to errors. For example, for uptake assessment in tumor biopsies it is difficult to take a representative part of the tumor. For PET assessment, partial volume effects will cause an underestimation of the tumor dose. This problem with partial volume effects is a known limitation of PET and correction methods are currently being developed to deal with this. At this point we can at least identify patients with low and high tumor uptake, respectively, and, therefore, it is possible to select the patients who may and may not benefit from therapy.

Although ^{89}Zr-immuno-PET can become an important tool in the detection and treatment of cancer, there are some limitations to overcome. Drawing of the organ VOI´s requires anatomical knowledge, training, and is time consuming.

However, with modern PET/CT scanners, ^{89}Zr-immuno-PET data can be collected along with a structural CT image in one scanning session. The aligned CT data can then be used for a more accurate and automated VOI definition.

The mean radiation dose for patients in this study was about 40 mSv, which is high and will limit repeated application of ^{89}Zr-immuno-PET. However, the introduction of the new generation PET/CT scanners will also make that better quality immuno-PET images can be obtained with the use of less ^{89}Zr radioactivity dose. This can be concluded from preliminary PET/CT studies in which 37 MBq ^{89}Zr-trastuzumab was used for HER2 immuno-PET imaging in breast cancer patients (*15*). Using ^{89}Zr-cmAb U36 in combination with these scanners would mean an effective dose of about 20 mSv for a whole body scan. Theoretically, shorter lived residualizing positron emitters like ^{64}Cu (t½ = 12.7 h) and ^{86}Y (t½ = 14.7 h) might give less dose exposure, although, clinical experience with these positron emitters is very limited. In a study of Cutler et al., immuno-PET with 370 MBq ^{64}Cu-labeled intact mAb 1A3 was evaluated for detection of colorectal cancer with a Siemens/CTI ECAT EXACT PET scanner as was also used in the present study (*31,32*). The average whole body dose for these patients was 11.1 mSv. However, due to the short half-life of ^{64}Cu, most of the patients had to be imaged within 24 h p.i. to obtain good quality images. As shown in Figure 1A, for cmAb U36 delineation of tumors is much better at later time points (72 and 144 h), and therefore, the use of ^{64}Cu might be a less suitable alternative. For immuno-PET evaluation of antibody fragments, however, ^{64}Cu as well as ^{86}Y might be suitable candidates.

CONCLUSION

In the present study we evaluated the use of immuno-PET with ^{89}Zr-labeled-cmAb U36 in HNSCC patients regarding safety, biodistribution, radiation dose, and the potential for quantification. ^{89}Zr-cmAb U36 was found to be safe and well tolerated in all subjects. Uptake of radioactivity in heart, lungs, liver, kidneys, and spleen was decreasing over time, while increased uptake was only seen at tumor sites and in the thyroid of some of the patients. Quantitative analysis, comparing PET derived bloodpool activity and sampled blood activity, showed good agreement except for the patients with a body weight above 100 kg. Also a good agreement was found for assessment of antibody uptake in tumors. The mean effective dose

for the whole body was 0.53 ± 0.03 mSv/MBq in males and 0.66 ± 0.03 mSv/MBq in females.

ACKNOWLEDGMENTS

This study was supported by the Dutch Cancer Society, grant number IKA VU2000-2155. This study was partly performed within the framework of CTMM, the Center for Translational Molecular Medicine (www.ctmm.nl), project AIRFORCE number 03O-103.

REFERENCES

1. Oldham RK, Dillman RO. Monoclonal antibodies in cancer therapy: 25 years of progress. *J Clin Oncol*. 2008;26:1774-1777.
2. Börjesson PKE, Jauw YWS, Boellaard R, et al. Performance of immuno-positron emission tomography with zirconium-89-labeled chimeric monoclonal antibody U36 in the detection of lymph node metastases in head and neck cancer patients. *Clin Cancer Res*. 2006;12:2133-2140.
3. Verel I, Visser GWM, Dongen GA van. The Promise of Immuno-PET in Radioimmunotherapy. *J Nucl Med*. 2005;46:164S-171S.
4. Dongen GAMS van, Visser GWM, Hooge MNL, Vries EG de, Perk LR. Immuno-PET: A Navigator in Monoclonal Antibody Development and Applications. *The Oncologist*. 2007;12:1379-1389.
5. Wu AM. Antibodies and Antimatter: The Resurgence of Immuno-PET. *J Nucl Med*. 2009;50:2-5.
6. Nayak TK, Brechbiel MW. Radioimmunoimaging with longer-lived positron-emitting radionuclides: potentials and challenges. *Bioconjug Chem*. 2009;20:825-841.
7. Verel I, Visser GWM, Boerman OC, et al. Long-lived positron emitters zirconium-89 and iodine-124 for scouting of therapeutic radioimmunoconjugates with PET. *Cancer Biother Radiopharm*. 2003;18:655-661.
8. Perk LR, Visser GWM, Vosjan MJWD, et al. 89Zr as a PET Surrogate Radioisotope for Scouting Biodistribution of the Therapeutic Radiometals 90Y and 177Lu in Tumor-Bearing Nude Mice After Coupling to the Internalizing Antibody Cetuximab. *J Nucl Med*. 2005;46:1898-1906.
9. Perk LR, Visser OJ, Stigter-van Walsum M, et al. Preparation and evaluation of (89)Zr-Zevalin for monitoring of (90)Y-Zevalin biodistribution with positron emission tomography. *Eur J Nucl Med Mol Imaging*. 2006;33:1337-1345.
10. Verel I, Visser GWM, Boellaard R, Walsum MS, Snow GB, Dongen GAMS van. 89Zr Immuno-PET: Comprehensive Procedures for the Production of 89Zr-Labeled Monoclonal Antibodies. *J Nucl Med*. 2003;44:1271-1281.
11. Perk LR, Stigter-van Walsum M, Visser GWM, et al. Quantitative PET imaging of Met-expressing human cancer xenografts with 89Zr-labelled monoclonal antibody DN30. *Eur J Nucl Med Mol Imaging*. 2008;35:1857-1867.
12. Brouwers A, Verel I, Van Eerd J, et al. PET radioimmunoscintigraphy of renal cell cancer using 89Zr-labeled cG250 monoclonal antibody in nude rats. *Cancer Biother Radiopharm*. 2004;19:155-163.
13. Nagengast WB, de Vries EG, Hospers GA, et al. In vivo VEGF imaging with radiolabeled bevacizumab in a human ovarian tumor xenograft. *J Nucl Med*. 2007;48:1313-1319.
14. Aerts HJWL, Dubois L, Perk L, et al. Disparity between in vivo EGFR expression and 89Zr-labeled cetuximab uptake assessed with PET. *J Nucl Med*. 2009;50:123-131.
15. Dijkers ECF, Kosterink JGW, Rademaker AP, et al. Development and characterization of clinical-grade 89Zr-trastuzumab for HER2/neu immunoPET imaging. *J Nucl Med*. 2009;50:974-981.
16. Bree R de, Roos JC, Quak JJ, Hollander W den, Snow GB, Dongen GA van. Radioimmunoscintigraphy and biodistribution of technetium-99m-labeled monoclonal antibody U36 in patients with head and neck cancer. *Clin Cancer Res*. 1995;1:591-598.
17. Colnot DR, Quak JJ, Roos JC, et al. Phase I Therapy Study of 186Re-Labeled Chimeric Monoclonal Antibody U36 in Patients with Squamous Cell Carcinoma of the Head and Neck. *J Nucl Med*. 2000;41:1999-2010.
18. De Bree R, Roos JC, Quak JJ, Den Hollander W, Snow GB, Van Dongen GA. Clinical screening of monoclonal antibodies 323/A3, cSF-25 and K928 for suitability of targetting tumours in the upper aerodigestive and respiratory tract. *Nucl Med Commun*. 1994;15:613-627.
19. Heider KH, Mulder JW, Ostermann E, et al. Splice variants of the cell surface glycoprotein CD44 associated with metastatic tumour cells are expressed in normal tissues of humans and cynomolgus monkeys. *Eur J Cancer*. 1995;31A:2385-2391.
20. Prince ME, Sivanandan R, Kaczorowski A, et al. Identification of a subpopulation of cells with cancer stem cell properties in head and neck squamous cell carcinoma. *Proc Natl Acad Sci USA*. 2007;104:973-978.

21. Mack B, Gires O. CD44s and CD44v6 expression in head and neck epithelia. *PLoS ONE*. 2008;3:e3360.
22. Boellaard R, Hoekstra O, Lammertsma A. Software tools for standardized analysis of FDG whole body studies in multi-center trials. *J Nucl Med*. 2008;49:159P-159P.
23. Stabin MG, Sparks RB, Crowe E. OLINDA/EXM: the second-generation personal computer software for internal dose assessment in nuclear medicine. *J Nucl Med*. 2005;46:1023-1027.
24. Sgouros G. Bone marrow dosimetry for radioimmunotherapy: theoretical considerations. *J Nucl Med*. 1993;34:689-694.
25. Plaizier MA, Roos JC, Teule GJ, et al. Comparison of non-invasive approaches to red marrow dosimetry for radiolabelled monoclonal antibodies. *Eur J Nucl Med*. 1994;21:216-222.
26. Jones WF, Digby WM, Luk WK, Casey ME, Byars LG. Optimizing rod window width in positron emission tomography. *IEEE Trans Med Imaging*. 1995;14:266-270.
27. Tatsumi M, Clark PA, Nakamoto Y, Wahl RL. Impact of body habitus on quantitative and qualitative image quality in whole-body FDG-PET. *Eur J Nucl Med Mol Imaging*. 2003;30:40-45.
28. Botkin CD, Osman MM. Prevalence, challenges, and solutions for (18)F-FDG PET studies of obese patients: a technologist's perspective. *J Nucl Med Technol*. 2007;35:80-83.
29. Halpern BS, Dahlbom M, Quon A, et al. Impact of patient weight and emission scan duration on PET/CT image quality and lesion detectability. *J Nucl Med*. 2004;45:797-801.
30. Halpern BS, Dahlbom M, Auerbach MA, et al. Optimizing imaging protocols for overweight and obese patients: a lutetium orthosilicate PET/CT study. *J Nucl Med*. 2005;46:603-607.
31. Philpott GW, Schwarz SW, Anderson CJ, et al. RadioimmunoPET: detection of colorectal carcinoma with positron-emitting copper-64-labeled monoclonal antibody. *J Nucl Med*. 1995;36:1818-1824.
32. Cutler PD, Schwarz SW, Anderson CJ, et al. Dosimetry of copper-64-labeled monoclonal antibody 1A3 as determined by PET imaging of the torso. *J Nucl Med*. 1995;36:2363-2371.